JGR Space Physics

RESEARCH ARTICLE
10.1029/2020JA028067

Dynamics of Auroral Precipitation Boundaries Associated With STEVE and SAID

Y. Nishimura[1], E. F. Donovan[2], V. Angelopoulos[3], and N. Nishitani[4]

[1]Department of Electrical and Computer Engineering and Center for Space Physics, Boston University, Boston, MA, USA, [2]Department of Physics and Astronomy, University of Calgary, Calgary, Alberta, Canada, [3]Department of Earth, Planetary and Space Sciences, University of California, Los Angeles, CA, USA, [4]Institute for Space Earth Environmental Research, Nagoya University, Nagoya, Japan

This article is a companion to Nishimura et al. (2020), https://doi.org/10.1029/2020JA027782.

Key Points:
- STEVE events are associated with a sharper electron flux gradient, weaker ion precipitation, and a narrower gap of ions and electrons
- The narrow gap contains intense SAID, upflow, localized downward R2 FACs, trough, and elevated electron temperature
- Subauroral flows and downward FACs can only flow within the narrow gap, resulting in intense SAID and heating

Supporting Information:
- Supporting Information S1
- Movie S1
- Movie S2

Correspondence to:
Y. Nishimura,
toshi16@bu.edu

Citation:
Nishimura, Y., Donovan, E. F., Angelopoulos, V., & Nishitani, N. (2020). Dynamics of auroral precipitation boundaries associated with STEVE and SAID. *Journal of Geophysical Research: Space Physics*, *125*, e2020JA028067. https://doi.org/10.1029/2020JA028067

Received 31 MAR 2020
Accepted 15 MAY 2020
Accepted article online 19 JUN 2020

Abstract Using Defense Meteorological Satellite Program (DMSP) and National Oceanic and Atmospheric Administration (NOAA) satellite observations and ground-based observations by the THEMIS all-sky imagers (ASIs) and SuperDARN radars, we determine how the equatorward boundary locations of ring current ions and plasma sheet electrons at pre-midnight relate to occurrence of strong thermal emission velocity enhancement (STEVE) and intense subauroral ion drifts (SAID) during substorms. We found that the STEVE events are associated with a sharper gradient of electron precipitating flux, lower precipitating ion flux, and a narrower (<1°) latitudinal gap between the equatorward boundaries of trapped ring current ions and precipitating plasma sheet electrons and narrower region-2 field-aligned currents (FACs) than for the non-STEVE events. The narrow gap of the particle boundaries contains intense SAID, higher upflow velocity, lower trough density, and slightly higher electron temperature than those for the non-STEVE events. The non-STEVE substorms have much wider gaps between the trapped ions and precipitating electrons, and subauroral polarization streams (SAPS) do not show intense SAID. These results indicate that subauroral flows and downward FACs for the STEVE events can only flow within the latitudinally narrow subauroral low-conductance region between the ion and electron boundaries, resulting in intense SAID and heating. During the non-STEVE events, the SAPS flows can flow in the latitudinally wide region without forming intense SAID.

Plain Language Summary We show that STEVE (strong thermal emission velocity enhancement) is closely related to unusual structures of energetic ion and electron structures. Usually, energetic ions extend a few degrees equatorward of energetic electrons, and a moderate plasma jet stream is located between them. Interestingly, during STEVE, the gap between ions and electrons narrows down below 1°, and the electron flux falls off much more sharply. The plasma jet stream is confined between the ion-electron boundaries, and the velocity increases an order of magnitude higher. We suggest that the narrow particle boundaries are created by unusual particle injection to the near-Earth region and form the narrow flow channel that contributes to waves and plasma heating.

1. Introduction

Strong thermal emission velocity enhancement (STEVE) is an arc-like optical emission in the pre-midnight subauroral ionosphere (MacDonald et al., 2018). STEVE occurs during the recovery phase of substorms (Gallardo-Lacourt, Nishimura, et al., 2018), and STEVE is associated with intense subauroral ion drifts (SAID) (Archer et al., 2019; MacDonald et al., 2018; Nishimura et al., 2019). Satellite observations in the inner magnetosphere showed that the SAID flow channel occurs in a narrow radial separation between the sharp flux gradients of plasma sheet electrons and ring current ions, and electron precipitation and heating by the fast flow and waves have been suggested to be the inner magnetospheric structures that drive STEVE (Nishimura et al., 2019).

Gallardo-Lacourt, Nishimura, et al. (2018) also showed that STEVE is a rare phenomenon, with only a few events per year in North America. Even by considering that some events were missed due to limited sky conditions, STEVE is much less common than substorms despite that STEVE occurs during substorms. The low occurrence of STEVE indicates that a certain type of substorms possesses unusual conditions that drive STEVE. The occurrence during the substorm recovery phase also suggests that the magnetosphere-ionosphere system during the recovery phase contains unique conditions rather than just a simple

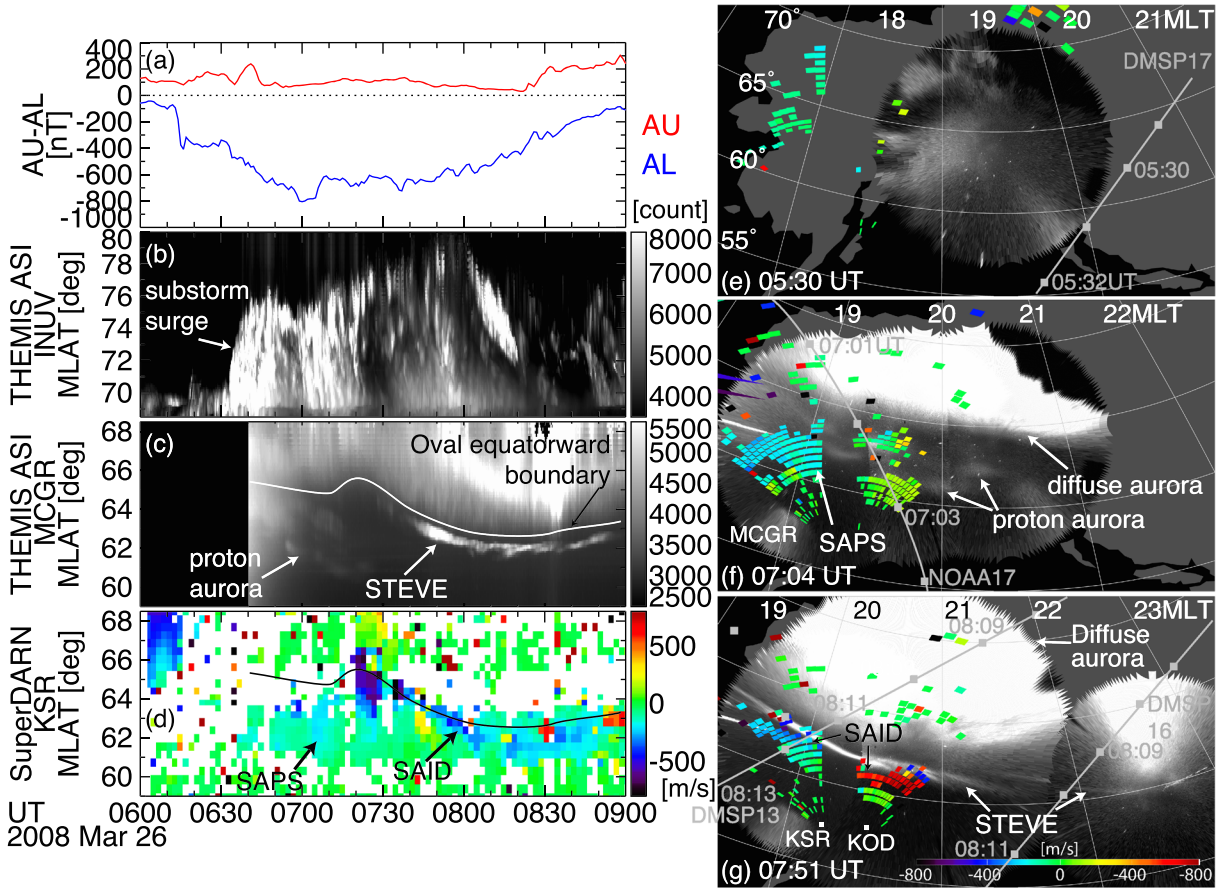

Figure 1. A substorm event on 26 March 2008. (a) *AU* and *AL* indices, THEMIS ASI keograms at (b) Inuvik (INUV) and (c) McGrath (MCGR, turned on at 6:40 UT), (d) SuperDARN LOS velocity data at Kodiak (KOD), and (e–g) imager and SuperDARN (KOD and King Salmon [KSR]) snapshots at 5:30 (before substorm), 7:04 (expansion phase), and 7:51 UT (recovery phase) together with DMSP and NOAA satellite orbits closest to the snapshot times. The snapshot times in panels (e) and (f) were chosen for presenting best available radar echo coverage. The solid lines in panels (c) and (d) mark the equatorward boundary of the auroral oval. See Movie S1 to see the whole time sequence of the 2-D images.

decaying phase of the system disturbance. Since STEVE is associated with SAID that are more intense than typical SAID, an investigation of the occurrence conditions of STEVE contributes to understanding of formation that the magnetosphere-ionosphere system favors intense SAID rather than weak SAID or latitudinally wider subauroral polarization stream (SAPS) without SAID.

Our companion paper (Nishimura et al., 2020) addresses these questions using measurements by magnetospheric satellites, auroral imaging, and currents. They showed that a large duskward propagation of the auroral surge and particle injection location sets up a favorable condition for SAID. A formation of SAID is important for extreme ionosphere heating that would drive STEVE emission. In the present study, we show evolution of the equatorward boundaries of precipitating and trapped particles at pre-midnight, using Defense Meteorological Satellite Program (DMSP) and National Oceanic and Atmospheric Administration (NOAA) Polar-orbiting Operational Environmental Satellite (POES) satellite measurements. Plasma drift measurements by DMSP and Super Dual Auroral Radar Network (SuperDARN) are also used to identify how the boundary evolution is related to SAID. Events with and without STEVE are compared, and differences in the particle boundary features are used to deduce magnetospheric conditions that favor STEVE and SAID occurrence. We show that the latitudinal separation between trapped ring current ions and plasma sheet electrons at pre-midnight is much narrower during the STEVE events, and intense SAID occurs between the narrow latitudinal separation of the particle boundaries. For the non-STEVE events, the separation remains latitudinally wide, and the subauroral flows also remain wide. We suggest that the latitudinal separation of the particle boundaries is strongly connected to the STEVE occurrence.

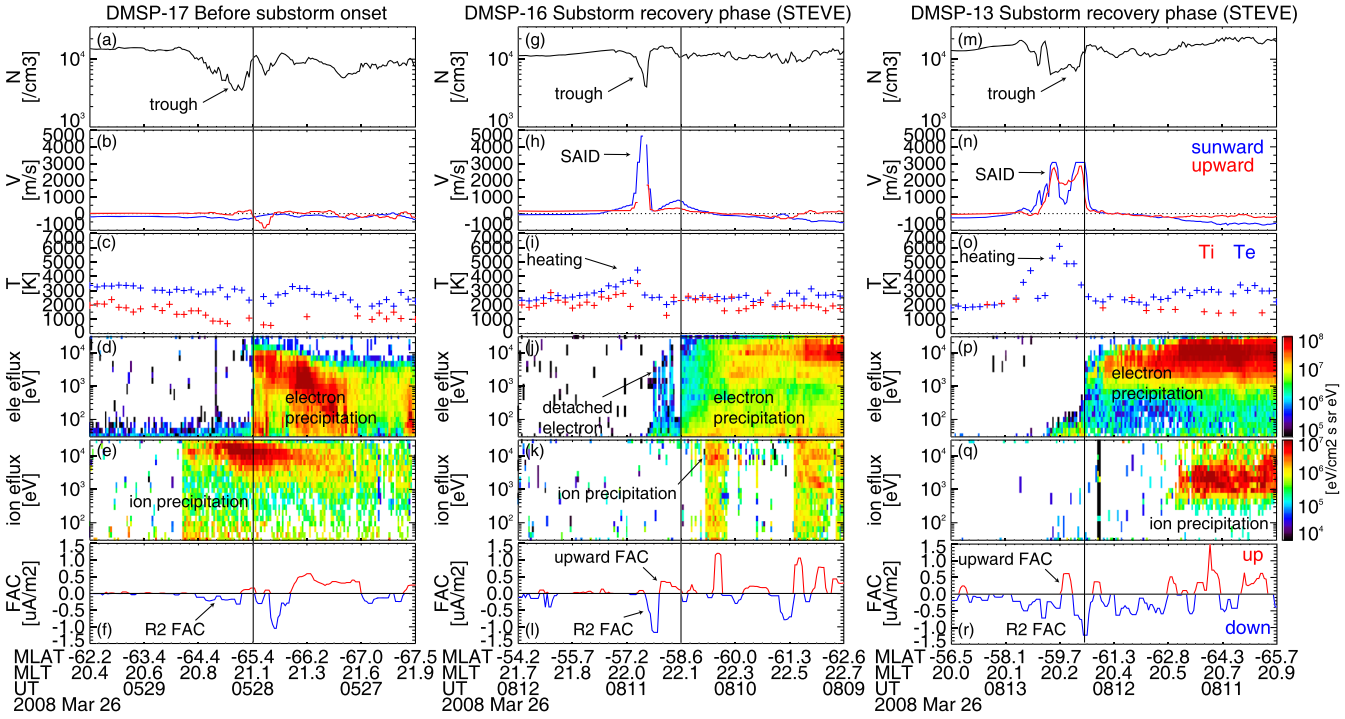

Figure 2. DMSP satellite data for the Figure 1 event. (a–f) DMSP-17 before the substorm, (g–l) DMSP-16 during STEVE, and (m–r) DMSP-13 during STEVE. From top to bottom, the panels shown are the density, cross-track velocity (blue: sunward; red: upward), temperature (blue: electron; red: ion), electron and ion precipitating energy fluxes, and FACs derived from the magnetic field (positive upward).

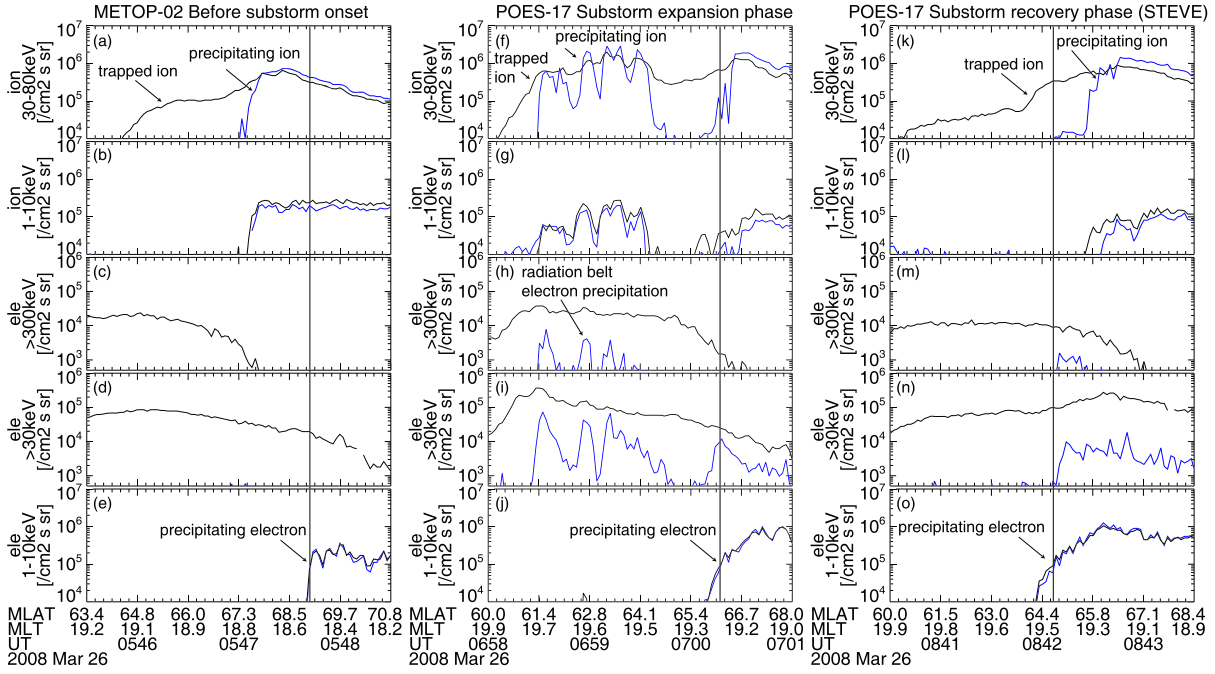

Figure 3. NOAA satellite data for the Figure 1 event. (a–e) METOP-02 before the substorm, (f–j) NOAA-17 before STEVE during the expansion phase, and (k–o) NOAA-17 during STEVE. From top to bottom, the panels shown are the 30–80 keV proton flux, >300 keV electron flux, and 1–10 keV electron flux. The blue and black lines show the precipitating and trapped particles. The vertical lines indicate the 1–10 keV electron equatorward boundary, at ~10^5 (/cm^2 s sr).

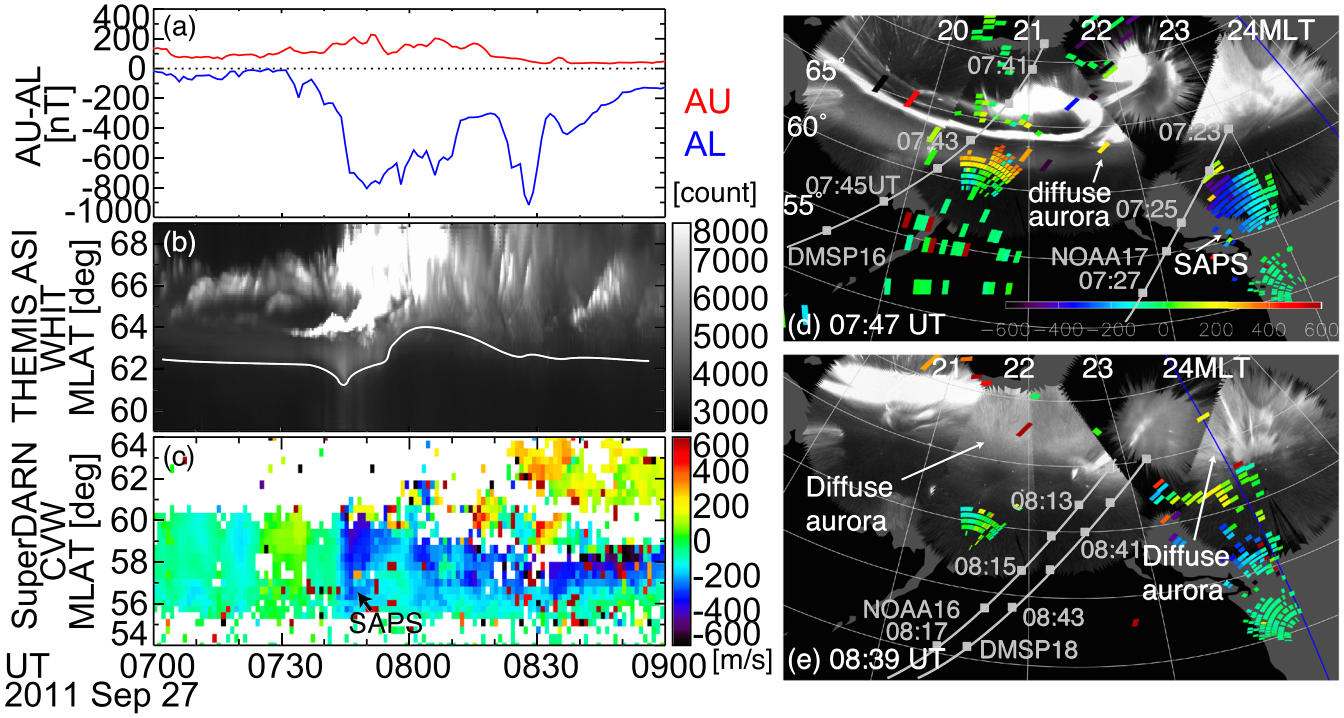

Figure 4. A substorm event with a similar *AL* magnitude but without STEVE on 27 September 2011. (a) *AU* and *AL* indices, (b) THEMIS ASI keogram at Whitehorse (WHIT), (c) SuperDARN LOS velocity at Christmas Valley West (CVW), and (d-e) snapshots of the THEMIS ASI data at 8:04 and 8:39 UT. The snapshot times in panels (d) and (e) were chosen for presenting best available radar echo coverage. The blue line marks the magnetic midnight. See Movie S2 to see the whole time sequence of the 2-D images.

2. Results

2.1. 26 March 2008 Event With STEVE

Figure 1 shows aurora and SuperDARN data of the 6–9 UT substorm on 26 March 2008 with a peak *AL* index of approximately −800 nT. Nishimura et al. (2020) also present this event with an emphasis on the surge and current evolution. During the expansion phase, the keograms from the imagers in Alaska (20–21 MLT) show a large poleward expansion when a surge passed over Alaska (Figure 1b) and diffuse emission equatorward of the auroral oval (Figures 1c and 1e, 19–20 MLT). As shown in Figure 3, this is driven by ion precipitation equatorward of plasma sheet electrons (i.e., proton aurora). During the recovery phase, a narrow arc appeared equatorward of diffuse aurora at ~07:22–09:00 UT, which is a STEVE arc. Colored photographs by a citizen scientist during this event show a mauve-colored arc equatorward of green diffuse aurora (http://www.spaceweather.com/aurora/gallery_01mar08_page4.htm). The SuperDARN line-of-sight (LOS) velocity data in the STEVE region show a latitudinally narrow westward flow (SAID, Figure 1d). Figure 1g shows that the SAID flow channel was aligned with the STEVE arc right equatorward of the arc. Considering that the KOD radar (looking northeast) detected velocity toward the radar and that the KSR radar (looking northwest) detected velocity away from the radar, the flows are predominantly directed westward.

Figure 2 shows DMSP data from three passes at pre-midnight before and during STEVE. Since these DMSP passes were in the Southern Hemisphere, we assume interhemispheric conjugacy and examine latitudinal structures relative to the electron equatorward boundary. As shown in Nishimura et al. (2020), STEVE was also detected in the Special Sensor Ultraviolet Spectrographic Imager (SSUSI) data in the Southern Hemisphere, and mapping at these L-shells is generally reliable due to dominance of the internal magnetic field. In addition, SAID was measured in both hemispheres (DMSP in the Southern Hemisphere and SuperDARN in the Northern Hemisphere), and this event occurred in equinox, where the conductance asymmetry is small. While conductance asymmetry could give differences in electric field structures (e.g., Kunduri et al., 2012), it is relevant to use the Southern Hemisphere measurements in this case.

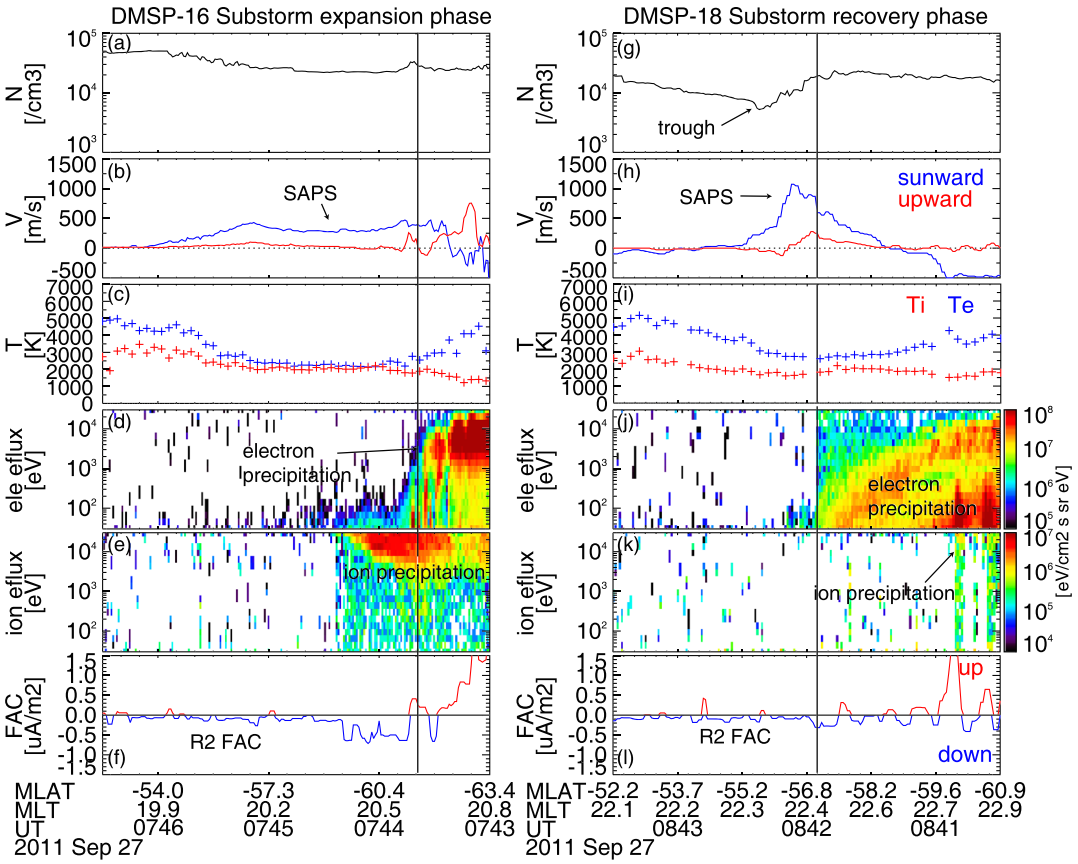

Figure 5. DMSP data for the Figure 4 event. (a–f) DMSP-16 during the substorm expansion phase and (g–l) DMSP-18 during the recovery phase. The format is the same as in Figure 2.

Before the substorm onset, ion precipitation extended equatorward of electron precipitation (Figures 2d and 2e), which is an ordinary particle structure at pre-midnight (Gussenhoven et al., 1987). The satellite did not detect any enhanced flow or temperature equatorward of the electron precipitation. Field-aligned currents (FACs) at those latitudes were mostly downward, typical region-2 (R2) FACs. During the substorm recovery phase, two satellites crossed STEVE as marked in Figure 1g and measured a latitudinally narrow sunward flow enhancement (SAID, Figures 2h and 2n), electron temperature enhancement (Figures 2i and 2o), and a pair of upward and downward FACs (Figures 2l and 2r) equatorward of the electron plasma sheet precipitation. The subauroral electron temperature enhancement is consistent with the report by Wang and Lühr (2013). The SAID was also collocated with a midlatitude trough (Figures 2g and 2m) and upflow (Figures 2h and 2n), consistent with the results by Anderson et al. (1993). In contrast to the measurements before the substorm, the ion precipitating flux substantially dropped and retreated poleward of the electron precipitation. The electron precipitation data also show a detached region of weak precipitation flux enhancement poleward of SAID (Figure 2j) and between the double SAID (Figure 2p). These features are consistent with the event in Nishimura et al. (2019).

Figure 3 shows the NOAA POES data at pre-midnight before and during STEVE. NOAA measurements are useful for investigating ions above 30 keV, where DMSP cannot detect. Before the substorm, >30 keV trapped and precipitating ions extended equatorward of 1–10 keV electrons (Figures 3a and 3e). The electrons are isotropic in all events we analyzed. NOAA-17 passed over the diffuse emission at 61–65° MLAT during the expansion phase and detected >30 keV precipitating ion flux enhancements equatorward of 1–10 keV electron flux (Figures 3f and 3j). Thus, the diffuse subauroral emission during the expansion phase is subauroral proton aurora. The enhanced proton precipitation was also associated with >300 keV radiation belt precipitating electron flux enhancements (Figure 3h), indicating electromagnetic ion cyclotron waves scattering ring current ions and radiation belt electrons. During STEVE in the substorm recovery phase,

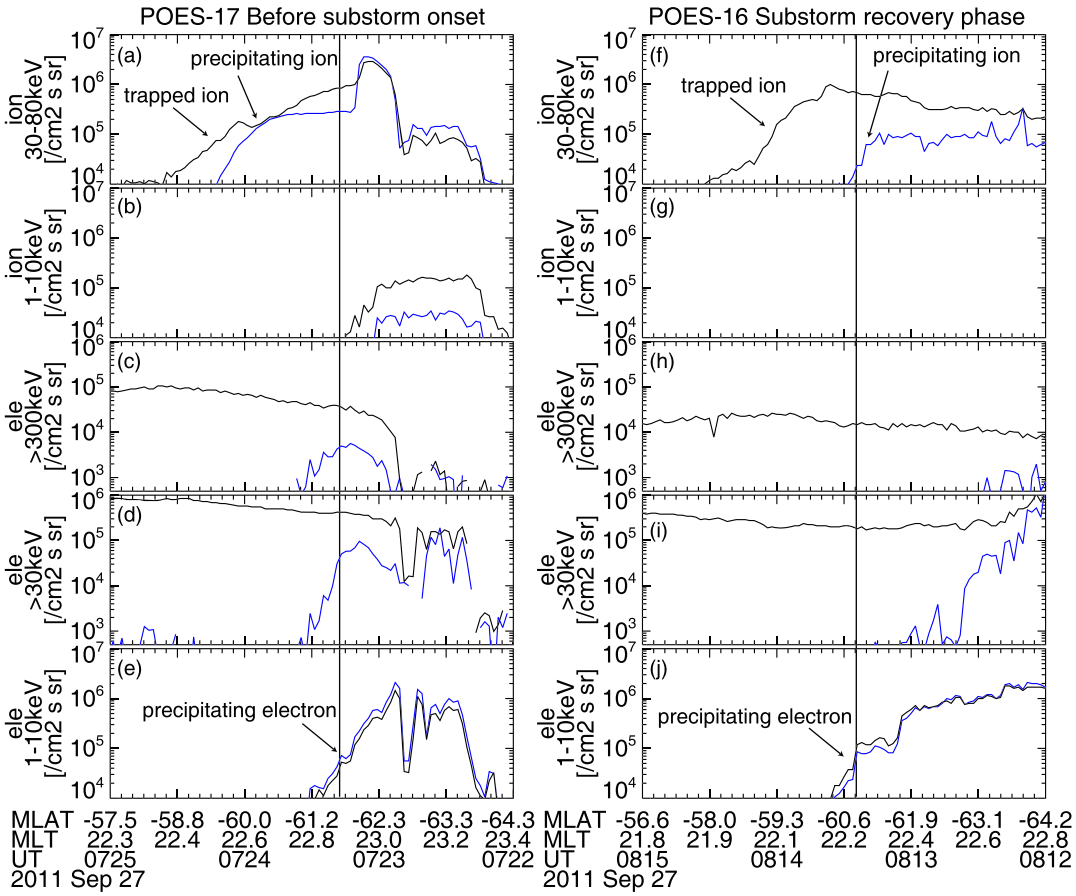

Figure 6. NOAA data for the Figure 4 event. (a–e) NOAA-17 before the substorm onset and (f–j) NOAA-16 during the recovery phase. The format is the same as in Figure 3.

the >30 keV ion precipitation was only found poleward of the 1–10 keV electron flux (Figures 3k and 3o). This is consistent with the STEVE event studied by Gallardo-Lacourt, Liang, et al. (2018). The >30 keV trapped ion flux also dropped within a degree equatorward of the electron precipitation, resulting in a much narrower gap between the trapped ions and precipitating electrons. The narrower separation between the trapped ions and plasma sheet electrons could explain why the subauroral flows are confined to a narrow latitude range (i.e., SAID), because that is the only region where the downward R2 FACs driven by the ring current could flow into the low conductance subauroral ionosphere. The >300 keV electron precipitation in the subauroral ionosphere also dropped below the noise level.

2.2. 27 September 2011 Event Without STEVE

We compare the low-altitude satellite measurements in section 2.1 STEVE event to those in a substorm event without STEVE. Figure 4 shows a substorm at 7:30–8:50 UT on 27 September 2011. Both this and section 2.1 events had a similar magnitude (peak *AL* approximately −800 nT) and occurred in the equinox at a similar UT range with a quiet preonset magnetic condition ($|AL| < 100$ nT). However, this event did not show a STEVE arc despite the good imager coverage in the pre-midnight subauroral ionosphere (Figures 4b, 4d, and 4e). The subauroral flow extends several degrees equatorward of the auroral equatorward boundary, and thus this is SAPS without SAID.

Figure 5 shows DMSP data for this event. During the expansion phase, the subauroral ionosphere showed a SAPS flow extending over ~7° MLAT (Figure 5b). Ion precipitation extended equatorward of electron precipitation. The FACs in the subauroral latitudes were downward. During the recovery phase, the SAPS flow velocity increased and became narrower (~3° latitude). The flow contains a localized peak, but it is much

Table 1
A List of Events Used in the Multievent Study

Date		DMSP				NOAA
yyyymmdd	STEVE	Flow type	Electron flux gradient	Te (K)	R2 FAC width	Ion-electron separation
20070905	Yes	SAID	Sharp	3700	0.4°	—
20080326	Yes	SAID	Sharp	4500	0.8°	1.0°
20080328	Yes	SAID	Sharp	4100	0.3°	—
20080412	Yes	SAID	Sharp	4400	0.4°	—
20100311	Yes	—	—	—	—	0.5°
20100405	Yes	SAID	Sharp	5000	0.6°	0.4°
20110402	Yes	SAID	Sharp	4700	0.3°	—
20160417	Yes	SAID	Sharp	—	2.4°	1.4°
20080201	No	SAPS	Gradual	3800	>4°	—
20080311	No	—	—	—	—	>4°
20080329	No	SAPS	Gradual	3300	2.2°	—
20100216	No	SAPS+SAID	Gradual	3700	1.8°	—
20100914	No	SAPS	Gradual	4100	>4°	—
20110303	No	SAPS	Gradual	3100	>4°	2.4°
20110927	No	SAPS	Gradual	2700	>4°	2.9°
20131030	No	SAPS	Gradual	4800	>4°	—

Note. The columns shown are the date, presence of STEVE, DMSP measurements of the flow type (with or without SAID), sharpness of the electron flux latitudinal gradient, electron temperature, R2 FAC latitudinal width, and NOAA measurements of trapped ion equatorward boundary location relative to the electron equatorward boundary. The "—" symbol denotes no observations.

weaker than the intense SAID flows associated with STEVE in Figure 2. The electron temperature did not show any enhancement within SAPS. The <30 keV ion precipitation was only found poleward of the electron equatorward boundary. The subauroral FACs were mostly downward without a localized peak or substantial upward FAC. In the STEVE event in Figures 2j and 2p, the energetic electron flux increased rapidly poleward of the electron equatorward boundary (the flux above 1 keV increased beyond 10^7 [eV/cm 2 s sr eV] within 0.7° from the electron equatorward boundary), but in Figure 4j, the energetic electron flux energy increased more gradually (~2° poleward). The electron energy also increased more gradually, indicating that energy-dependent magnetic drifts were more dominant in this event and >keV electrons did not reach the pre-midnight sector near the equatorward boundary of the auroral oval. In contrast, during the STEVE event in Figure 2, the energy dispersion is much smaller, and a substantial amount of >keV electrons reached the pre-midnight sector.

Figure 6 presents NOAA data at pre-midnight. Before the substorm onset, both trapped and precipitating >30 keV ions extended equatorward of 1–10 keV electrons (Figure 6a). During the recovery phase, the equatorward boundary of the precipitating >30 keV ions were close to that of the 1–10 keV electrons, while the trapped >30 keV ions extended >1.5° equatorward. This equatorward extension of the trapped ions is consistent with the broader latitudinal extent of the SAPS flow than in the section 2.1 event.

2.3. Multievent Study

We identified eight STEVE events detected by the THEMIS all-sky imagers (ASIs) where DMSP or NOAA footprints passed over STEVE. We require that the THEMIS ASIs detected substorm onset, auroral equatorward boundary and STEVE to place STEVE in the context of substorms and oval configuration. For comparison, we also selected eight substorms without STEVE in late winter or near equinox where the DMSP or NOAA satellites are available at pre-midnight. Those events are listed in Table 1. Using these events, we conducted a multievent study using the DMSP and NOAA data for examining whether the measured features described in sections 2.1 and 2.2 are repetitive among the multiple events. We sorted data by latitude relative to the equatorward boundary of the plasma sheet electrons, which is the sharpest flux gradient and typically at ~10^{11} (eV/cm^2 s sr) total energy flux at 30 eV to 30 keV for DMSP and ~10^5 (/cm^2 s sr) total number flux at 1–10 keV for NOAA. The use of the latitudes relative to the boundary is consistent with the approach used in past studies (Landry & Anderson, 2018; Wang & Lühr, 2013). We note that the number of events is small, and we do not intend that this is a large statistical study. Our key results are based on the panels with

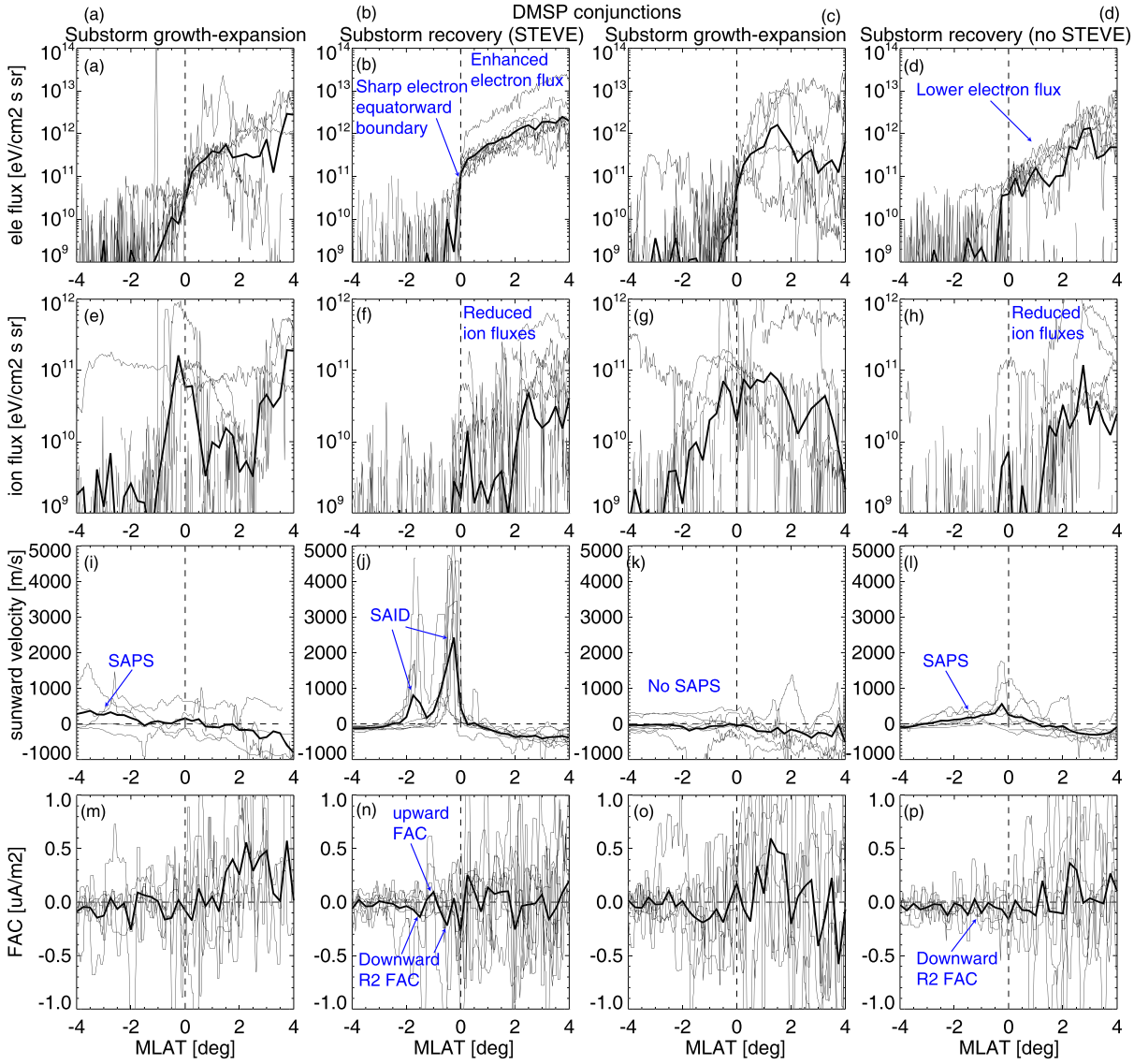

Figure 7. A multievent analysis of the DMSP data. From left to right, the columns shown are (A) STEVE events before the substorm recovery phase (before STEVE), (B) STEVE events during the recovery phase (during STEVE), (C) non-STEVE events before the recovery phase, and (D) non-STEVE events during the recovery phase. From top to bottom, the rows shown are (a–d) the total energy electron flux, (e–h) total ion energy flux, (i–l) sunward velocity, and (m–p) FAC. The epoch time is the electron equatorward boundary. The latitude is positive poleward. The thin lines show individual events, and the thick lines show the mean every 0.2° MLAT.

variances between the events are relatively small so that the trend is reliable. Other panels have larger variances between events and are not used to draw conclusions in this study.

The results are shown in Figures 7 and 8. The thick lines show the average every 0.2° latitude. The thin lines show individual satellite observations as an indicator of the error bar. The second and fourth columns in Figures 7 and 8 compare DMSP observations during the recovery phase of substorms with and without STEVE. The averaged profiles confirm the key features described in the previous sections. The events with STEVE on average have sharper electron flux gradient at the auroral equatorward boundary and larger precipitating electron flux within 2° from the boundary (Figures 7b and 7d), lower precipitating ion flux (Figures 7f and 7h), intense SAID (Figures 7j and 7l), more localized downward R2 FAC with a localized upward FAC equatorward of the electron precipitation (Figures 7n and 7p), pronounced upflow (Figures 8b and 8d), lower midlatitude-trough density (Figures 8f and 8h; most STEVE events show

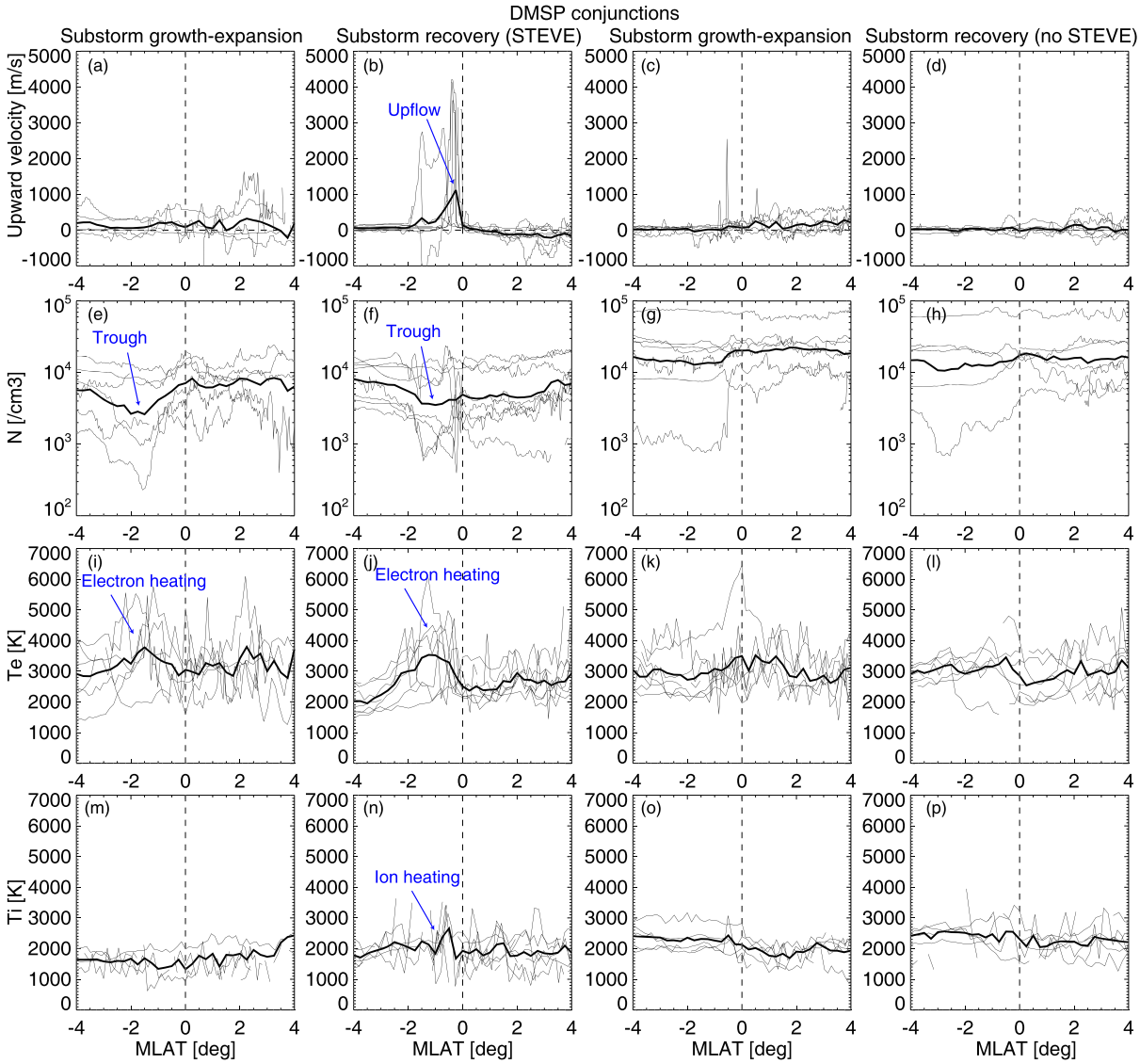

Figure 8. Same as Figure 7 except that the panels shown are (a–d) upward velocity, (e–h) ion density, (i–l) electron temperature, and (m–p) ion temperature.

minimum density reaching below 6,000 cm^{-3}, while only one non-STEVE event shows 6,000 cm^{-3} density), higher electron temperature (Figures 8j and 8l; most STEVE events show peak temperature of >4,000 K, while only two non-STEVE events reach >4,000 K), and slightly elevated ion temperature (Figures 8n and 8p; although the difference is not as evident as the other parameters) than those for the non-STEVE events. The key features are also summarized in Table 1. For the panels mentioned above, the average profiles mostly represent the behavior of the individual events. Outliers can be found (e.g., the highest curve in Figure 7b), but their presence do not affect the features mentioned above.

The STEVE events sometimes show a double SAID structure, while non-STEVE events tend to show weak SAPS flows of ~3° MLAT width without SAID (except for one event). The STEVE events are preceded by SAPS flows (Figure 7i), while non-STEVE events do not show significant preexisting SAPS flows. For non-STEVE events, the subauroral downward R2 FACs do not show a pronounced peak but spread wider in latitude than for the STEVE events. The non-STEVE events do not show notable upflows and temperature enhancements in the subauroral ionosphere. The trough during STEVE is deeper than that in non-STEVE events. But the trough is already present before STEVE (Figure 8e), and it is not clear if this is solely due

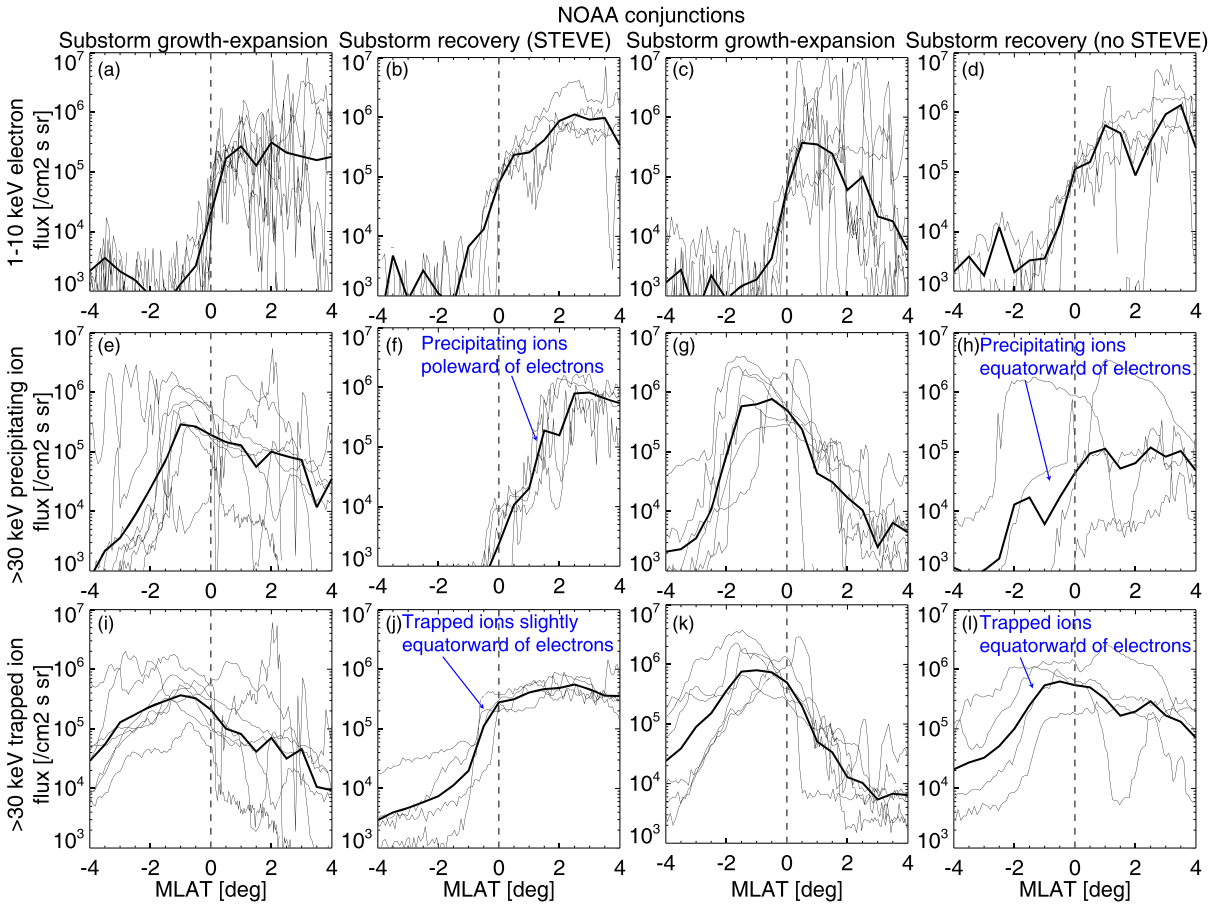

Figure 9. A multievent analysis of the NOAA data. Same as Figure 7 except that the panels shown are (a–d) 1–10 keV electron flux, (e–h) 30–80 keV precipitating ion flux, and (i–l) 30–80 keV trapped ion flux.

to STEVE or if it is related to the trough that existed before STEVE. The electron temperature during STEVE is on average larger than for non-STEVE events, but the temperature is already elevated before STEVE (Figure 8i), and the temperature enhancement extends over a few degrees, which are wider than STEVE and SAID. The electron heating may not be directly connected to the SAID but could be created by other processes that existed before the STEVE occurrence. The other parameters do not show substantial differences between the STEVE and non-STEVE events.

Figure 9 shows the NOAA data. The 1–10 keV flux profiles are similar for the STEVE and non-STEVE events (Figures 9b and 9d). In contrast, the >30 keV precipitating ion fluxes for the STEVE events drop poleward of the electron equatorward boundary (Figure 9f), while those for the non-STEVE events are more variable and on average extend equatorward of the electron equatorward boundary (Figure 9h). The >30 keV trapped ion fluxes for the STEVE events extend 1° equatorward of the electron equatorward boundary (Figure 9j), while those for the non-STEVE events extend >2° equatorward (Figure 9l).

3. Conclusion

We examined evolution of the equatorward boundaries of ions and electrons during STEVE using low-altitude satellites. By comparing to substorm events without STEVE, we found that the STEVE events are associated with a larger precipitating electron flux, sharper gradient of electron flux, lower precipitating ion flux, and a narrower gap between the equatorward boundaries of trapped ions and precipitating electrons. The narrow gap of the particle boundaries contains intense SAID, higher upflow velocity, localized downward R2 FACs, lower trough density, and higher electron temperature than those for the non-STEVE events.

The narrower gap between the trapped ring current ions and plasma sheet electrons during the STEVE events indicates that the downward R2 FACs from the ring current flows into the narrow region of the low-conductance subauroral ionosphere than for the non-STEVE events. The narrow gap explains why the subauroral flow channels during the STEVE events are narrow and fast, that is, forming SAID. The fast SAID flow and larger electron heating could contribute to the faster upflows. For the non-STEVE events, the trapped ions and plasma sheet electrons stay separated, and enhanced flows are latitudinally wide (SAPS without SAID). The narrower gap and sharper electron flux gradient during the STEVE events are consistent with the finding by Nishimura et al. (2020) that injection during STEVE events occur more preferentially at pre-midnight and brings more electron population to the inner magnetosphere. The earthward boundaries of the electrons and ions come close, and SAID forms in the narrow separation. The present study showed that their finding is supported by low-altitude satellite observations of particle boundaries and flows. We suggest that the narrow separation between the trapped ions and plasma sheet electrons is the key parameter for the occurrence of STEVE and SAID.

Data Availability Statement

The THEMIS, DMSP, NOAA, and SuperDARN data were obtained through themis.ssl.berkeley.edu, cdaweb.gsfc.nasa.gov, cedar.openmadrigal.org, www.ngdc.noaa.gov/stp/satellite/poes/dataaccess.html, and vt.superdarn.org. Data processing used SPEDAS V3.1 (Angelopoulos et al., 2019).

Acknowledgments

This work was supported by National Aeronautics and Space Administration (NASA) Grants NNX17AL22G and 80NSSC18K0657, National Science Foundation (NSF) Grants AGS-1907698, and Air Force Office of Scientific Research (AFOSR) FA9559-16-1-0364. The THEMIS mission and all-sky imagers are supported by NASA Contract NAS5-02099, Canadian Space Agency (CSA) Contract 9F007-046101, and NSF Grant AGS-1004736. We thank support from the CEDAR workshop "Grand Challenge: Multi scale I-T system dynamics" and ISSI workshop "Multi-Scale Magnetosphere-Ionosphere-Thermosphere Interaction".

References

Anderson, P. C., Hanson, W. B., Heelis, R. A., Craven, J. D., Baker, D. N., & Frank, L. A. (1993). A proposed production model of rapid subauroral ion drifts and their relationship to substorm evolution. *Journal of Geophysical Research*, *98*(A4), 6069–6078. https://doi.org/10.1029/92JA01975

Angelopoulos, V., Cruce, P., Drozdov, A., Grimes, E. W., Hatzigeorgiu, N., King, D. A., et al. (2019). *Space Science Reviews*, *215*(1), 9. https://doi.org/10.1007/s11214-018-0576-4

Archer, W. E., Gallardo-Lacourt, B., Perry, G. W., St. -Maurice, J.-P., Buchert, S. C., & Donovan, E. F. (2019). Steve: The optical signature of intense subauroral ion drifts. *Geophysical Research Letters*, *46*(12), 6279–6286. https://doi.org/10.1029/2019GL082687

Gallardo-Lacourt, B., Liang, J., Nishimura, Y., & Donovan, E. (2018). On the origin of STEVE: Particle precipitation or ionospheric skyglow? *Geophysical Research Letters*, *45*(16), 7968–7973. https://doi.org/10.1029/2018GL078509

Gallardo-Lacourt, B., Nishimura, Y., Donovan, E., Gillies, D. M., Perry, G. W., Archer, W. E., et al. (2018). A statistical analysis of STEVE. *Journal of Geophysical Research: Space Physics*, *123*, 9893–9905. https://doi.org/10.1029/2018JA025368

Gussenhoven, M. S., Hardy, D. A., & Heinemann, N. (1987). The equatorward boundary of auroral ion precipitation. *Journal of Geophysical Research*, *92*(A4), 3273–3283. https://doi.org/10.1029/JA092iA04p03273

Kunduri, B. S. R., Baker, J. B. H., Ruohoniemi, J. M., Clausen, L. B. N., Grocott, A., Thomas, E. G., et al. (2012). An examination of inter-hemispheric conjugacy in a subauroral polarization stream. *Journal of Geophysical Research*, *117*(A8), A08225. https://doi.org/10.1029/2012JA017784

Landry, R. G., & Anderson, P. C. (2018). An auroral boundary-oriented model of subauroral polarization streams (SAPS). *Journal of Geophysical Research: Space Physics*, *123*, 3154–3169. https://doi.org/10.1002/2017JA024921

MacDonald, E. A., Donovan, E. F., Nishimura, Y., Case, N. A., Gillies, D. M., Gallardo-Lacourt, B., et al. (2018). New science in plain sight: Citizen scientists lead to discovery of optical structure in the upper atmosphere. *Science Advances*, *4*(3), eaaq0030. https://doi.org/10.1126/sciadv.aaq0030

Nishimura, Y., Gallardo-Lacourt, B., Zou, Y., Mishin, E., Knudsen, D. J., Donovan, E. F., et al. (2019). Magnetospheric signatures of STEVE: Implications for the magnetospheric energy source and interhemispheric conjugacy. *Geophysical Research Letters*, *46*, 5637–5644. https://doi.org/10.1029/2019GL082460

Nishimura, Y., Yang, J., Weygand, J. M., Wang, W., Kosar, B., Donovan, E. F., et al. (2020). Magnetospheric conditions for STEVE and SAID: Particle injection, substorm surge and field-aligned currents. *Journal of Geophysical Research: Space Physics*, *125*, e2020JA027782. https://doi.org/10.1029/2020JA027782

Wang, H., & Lühr, H. (2013). Seasonal variation of the ion upflow in the topside ionosphere during SAPS (subauroral polarization stream) periods. *Annales de Geophysique*, *31*(9), 1521–1534. https://doi.org/10.5194/angeo-31-1521-2013